Supporting Information for

Boosting and stabilizing oxygen evolution reaction through Ru single atoms anchored amorphous $NiMoO_x$ electrocatalyst

Li *et al.*

Supplementary Figures

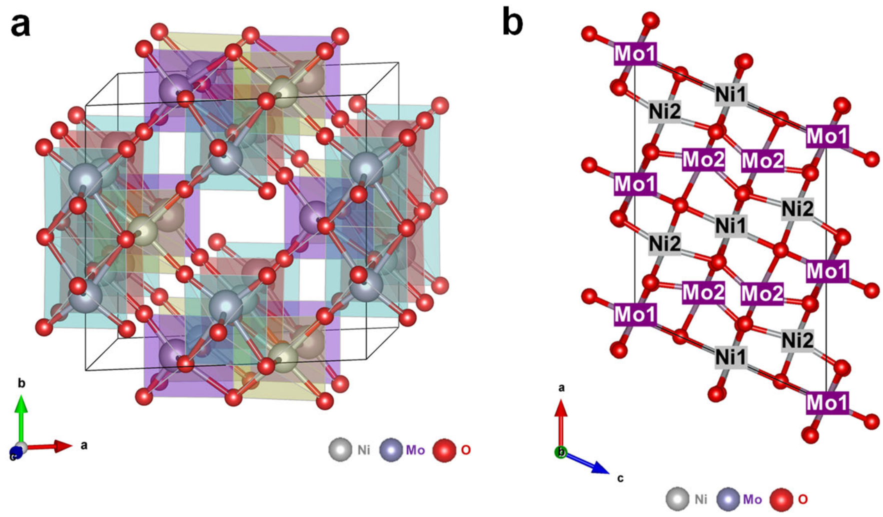

Supplementary Figure 1. Top view (**a**) and side view (**b**) of crystalline $NiMoO_4$ structure (PDF#33-0948).

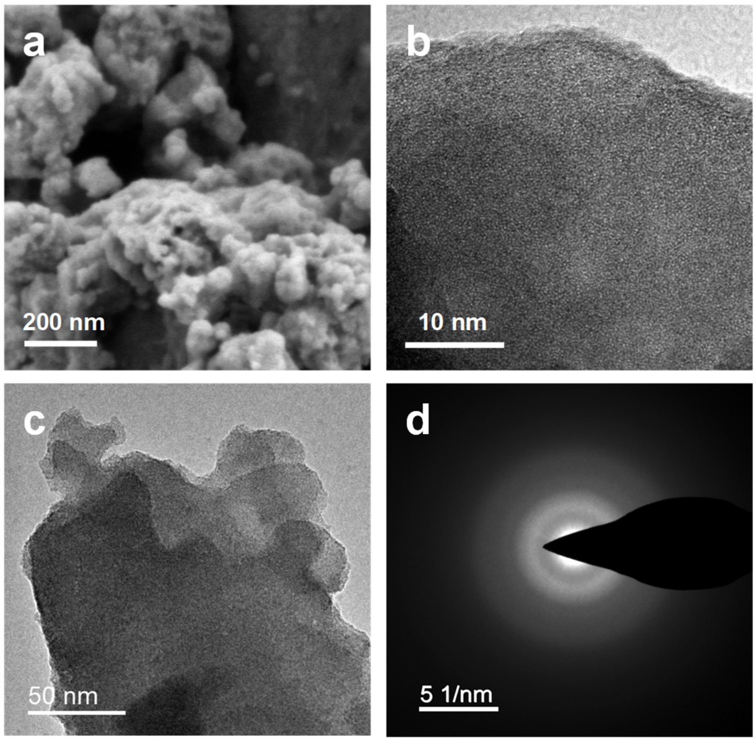

Supplementary Figure 2. (**a**) SEM, (**b, c**) HR-TEM and (**d**) SAED images of a-RNMO.

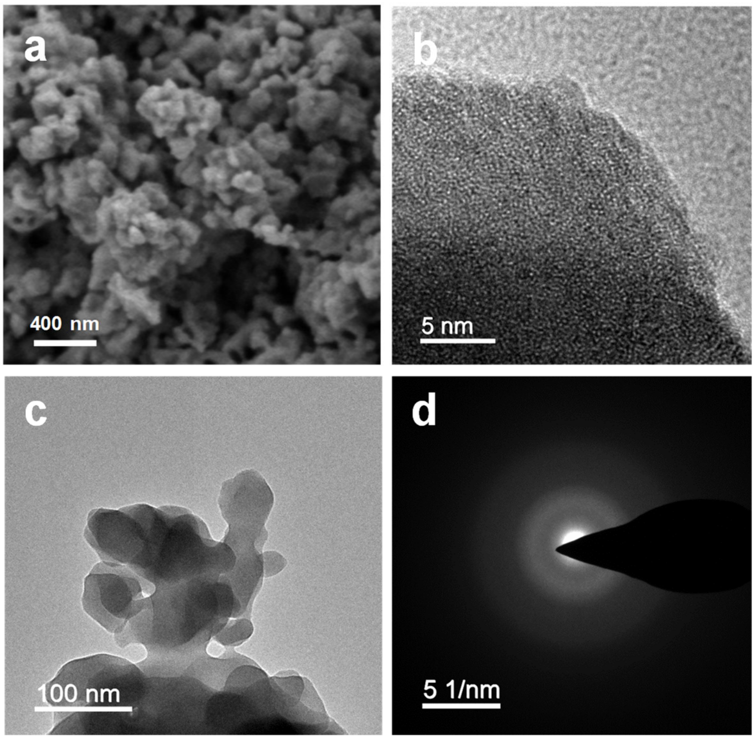

Supplementary Figure 3. (**a**) SEM, (**b, c**) HR-TEM and (**d**) SAED images of a-NMO.

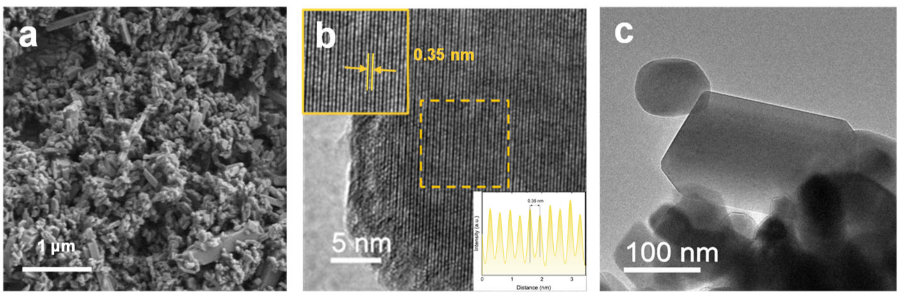

Supplementary Figure 4. (**a**) SEM, (**b, c**) HR-TEM images of c-NMO.

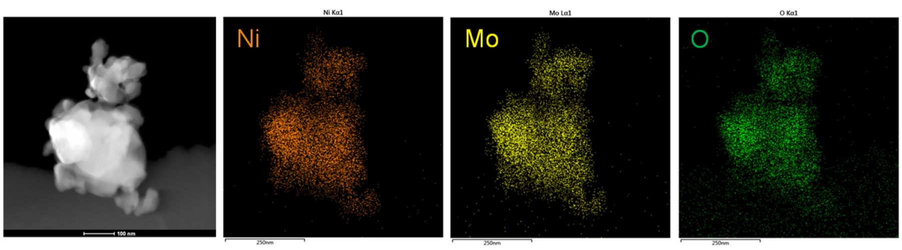

Supplementary Figure 5. EDS-mapping of a-NMO.

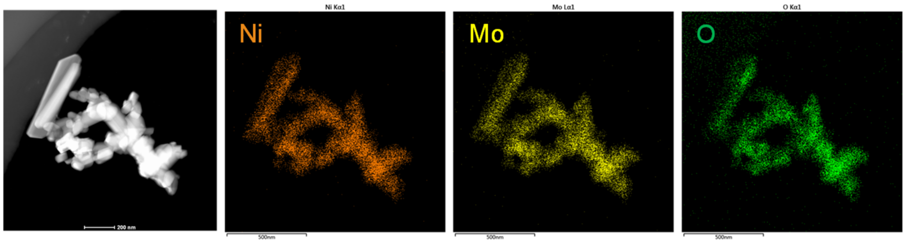

Supplementary Figure 6. EDS-mapping of c-NMO.

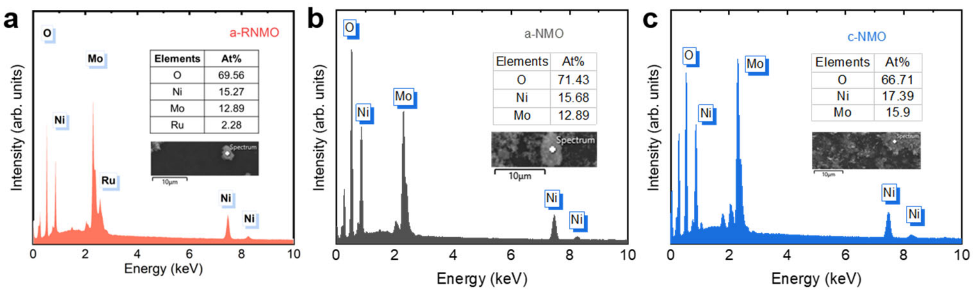

Supplementary Figure 7. SEM-EDS spectrum of (**a**) a-RNMO, (**b**) a-NMO, and (**c**) c-NMO. Source data are provided as a Source Data file.

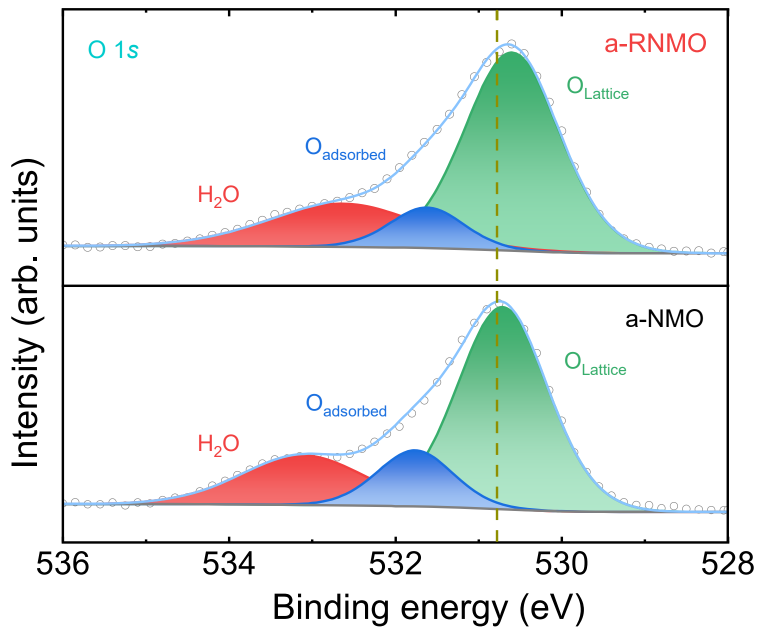

Supplementary Figure 8. O 1*s* XPS spectra of a-NMO and a-RNMO. Source data are provided as a Source Data file.

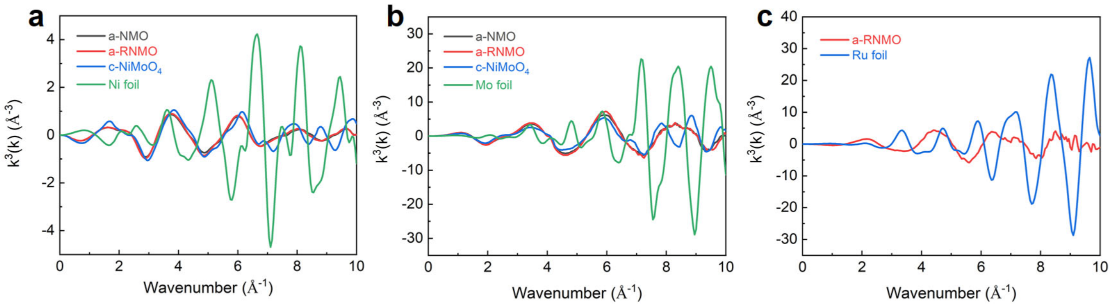

Supplementary Figure 9. The k^3-weighted k-space of (**a**) Ni *K*-edge, (**b**) Mo *K*-edge, and (**c**) Ru *K*-edge experimental spectra of a-NMO, a-RNMO, and references. Source data are provided as a Source Data file.

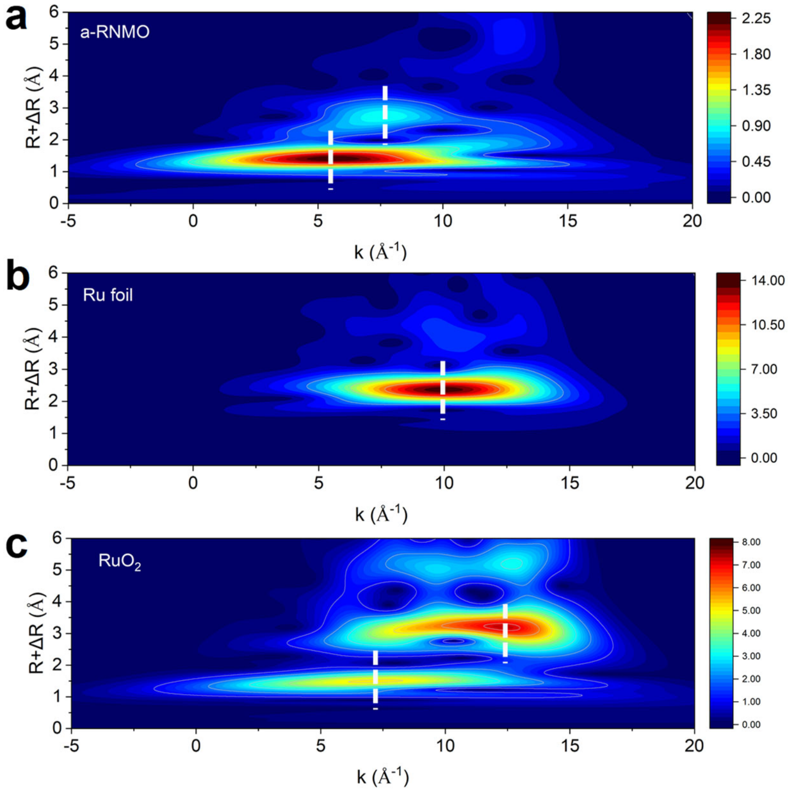

Supplementary Figure 10. WT-EXAFS analysis of Ru *K*-edge of (**a**) a-RNMO, (**b**) Ru foil, and (**c**) RuO_2. Source data are provided as a Source Data file.

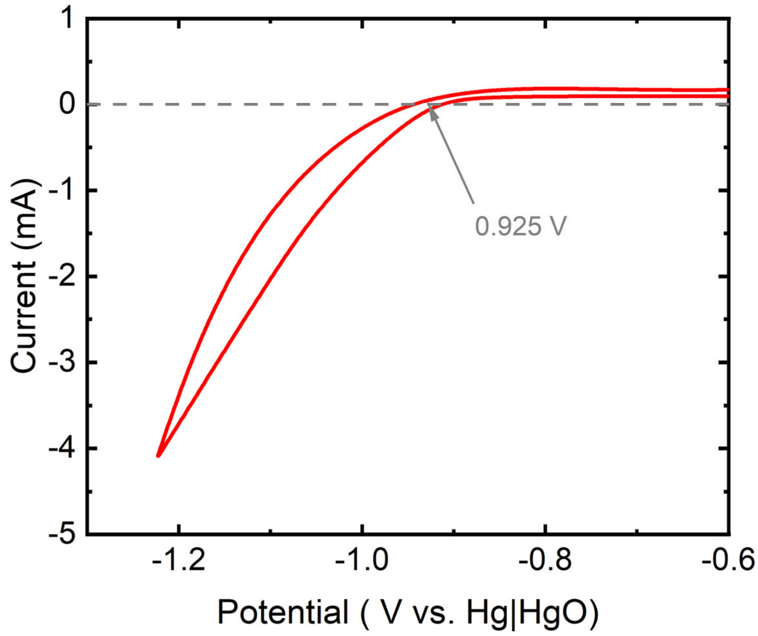

Supplementary Figure 11. Potential (without iR compensation) calibration of the Hg|HgO reference electrode in H_2-saturated 1 M KOH solution at 25 °C. Source data are provided as a Source Data file.

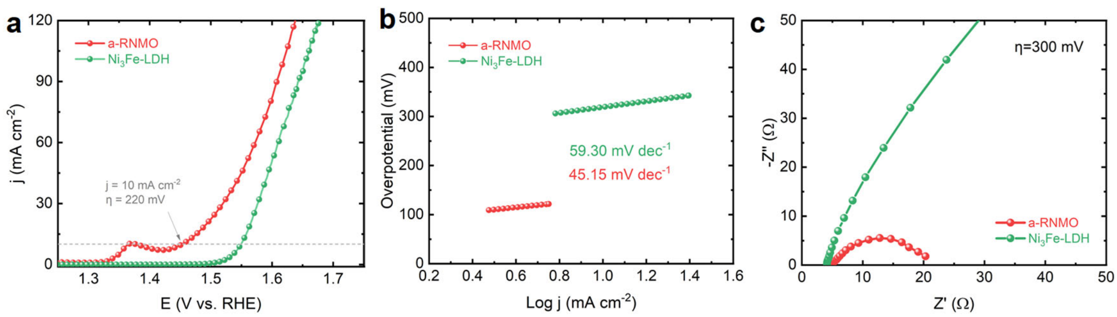

Supplementary Figure 12. Electrochemical performance of a-RNMO and NiFe-LDH. (a) LSV polarization curves. (b) Tafel plots extracted from (a). (c) EIS Nyquist plots. Source data are provided as a Source Data file.

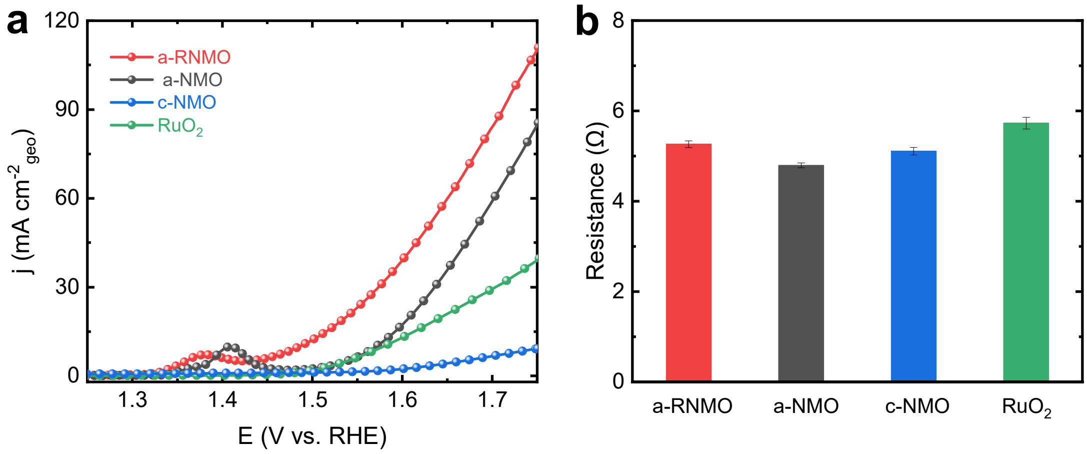

Supplementary Figure 13. (**a**) LSV polarization curves without iR-compensation of a-RNMO, a-NMO, c-NMO, and RuO_2 in 1 M KOH under 25 °C, at scan rate of 5 mV s^{-1}, using RDE (0.196 cm^2) with 1600 rpm. (**b**) The detected resistance for these electrocatalysts. Note: error bars represent the standard deviation of three independent measurements. Source data are provided as a Source Data file.

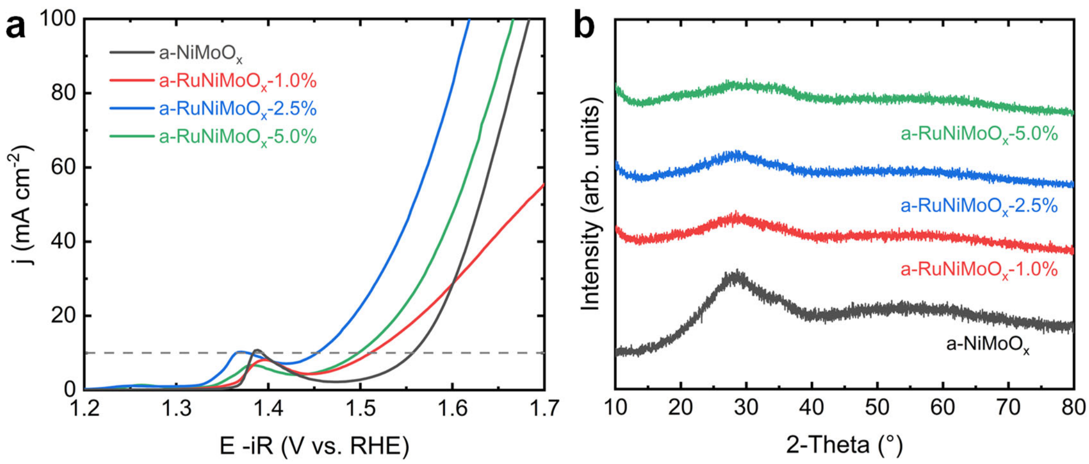

Supplementary Figure 14. (**a**) LSV polarization curves with iR-compensation with different Ru content, including at. % = 0%, 1%, 2.5%, 5%. (**b**) XRD patterns of them. Source data are provided as a Source Data file.

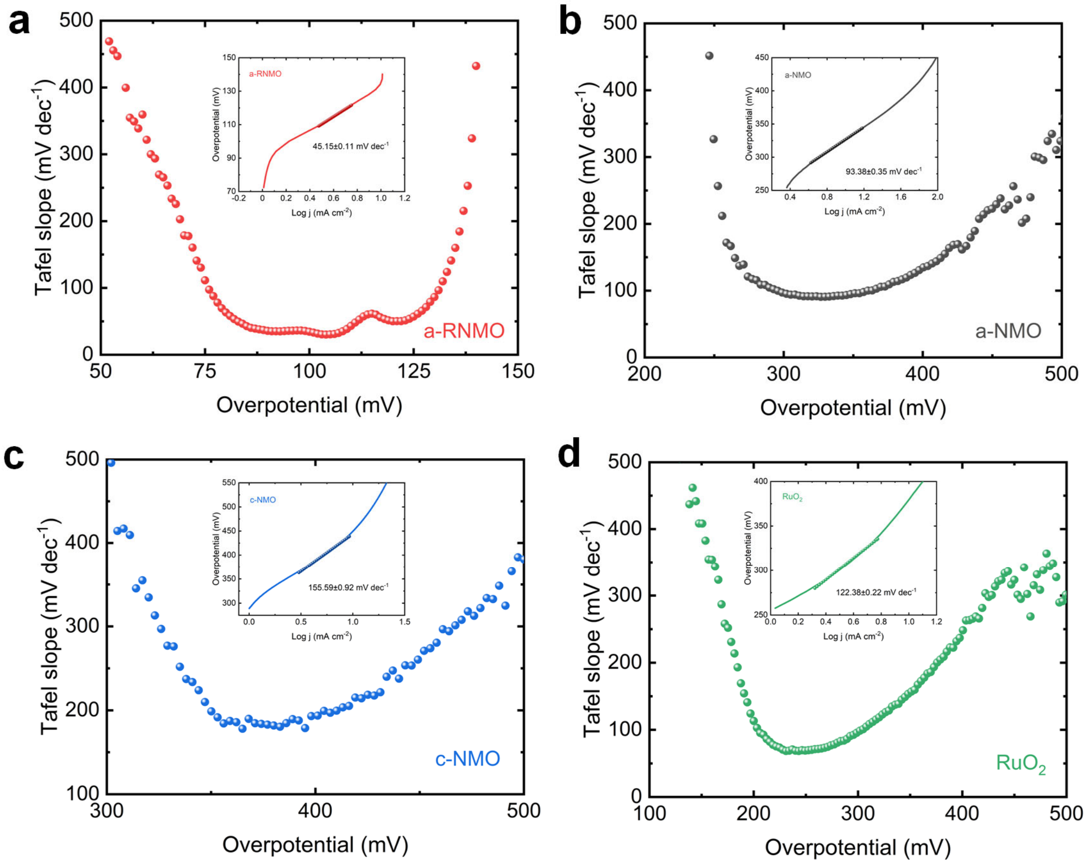

Supplementary Figure 15. The graphs that plot Tafel slope as a function of overpotential on (**a**) a-RNMO, (**b**) a-NMO, (**c**) c-NMO, and (**d**) RuO_2. Inset: The Tafel plots of these catalysts. Source data are provided as a Source Data file.

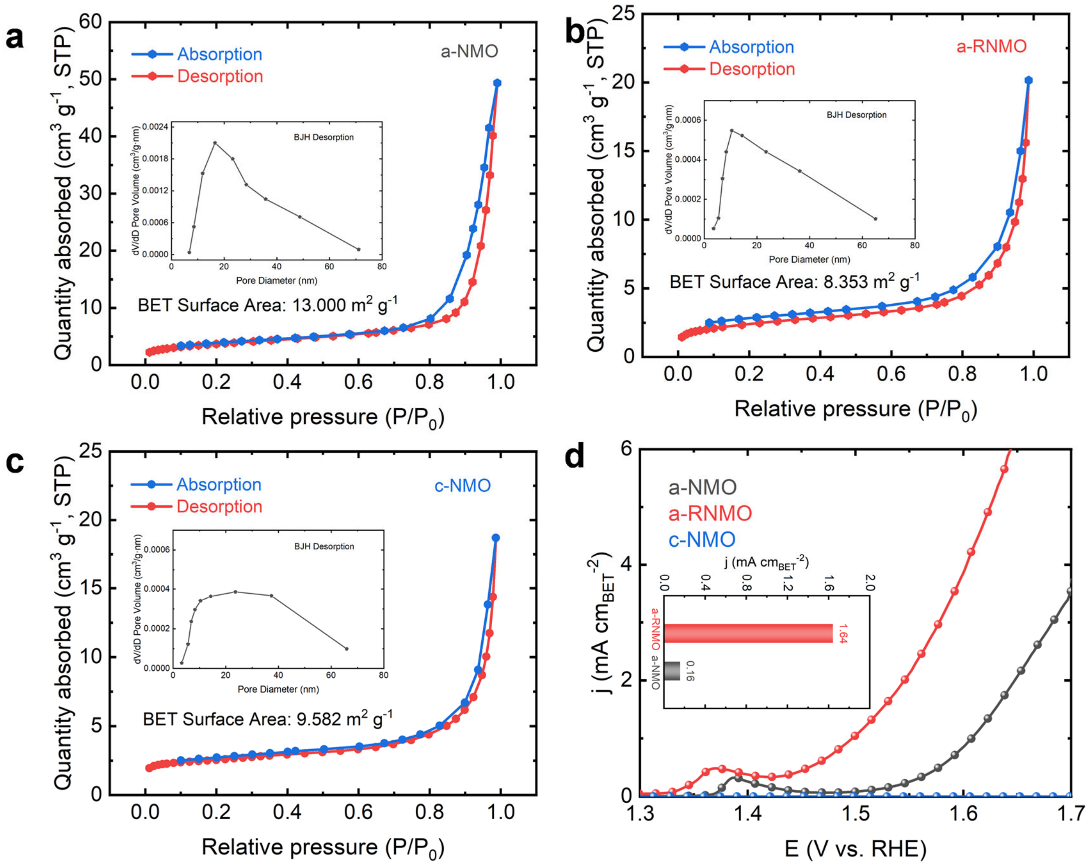

Supplementary Figure 16. N_2 absorption and desorption isotherms of (**a**) a-NMO, (**b**) a-RNMO, and (**c**) c-NMO. (**d**) LSV polarization curves normalized to BET specific areas of a-NMO, a-RNMO, and c-NMO. Inset: The normalized current density values of a-NMO and a-RNMO at 1.53 V vs. RHE. Source data are provided as a Source Data file.

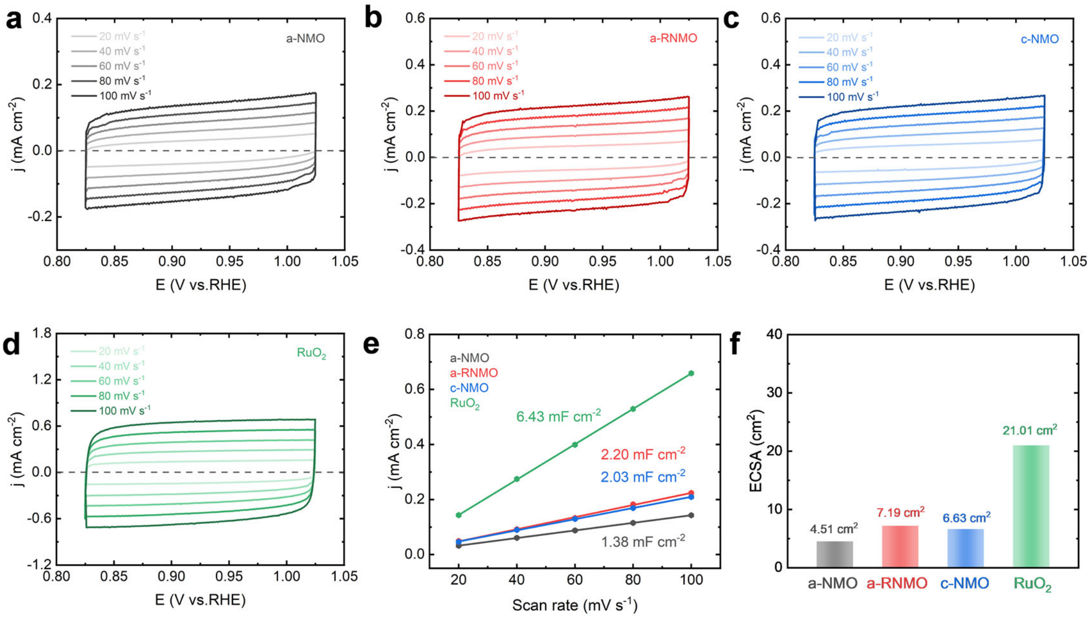

Supplementary Figure 17. Electrochemical CV scans at non-Faradic current for (**a**) a-NMO, (**b**) a-RNMO, (**c**) c-NMO, and (**d**) RuO_2, with 20, 40, 60, 80, and 100 mVs^{-1} scan rates. (**e**) linear fitting between the capacitive currents and CV scan rates for these electrocatalysts. (**f**) The ECSA values calculated for these electrocatalysts. Source data are provided as a Source Data file.

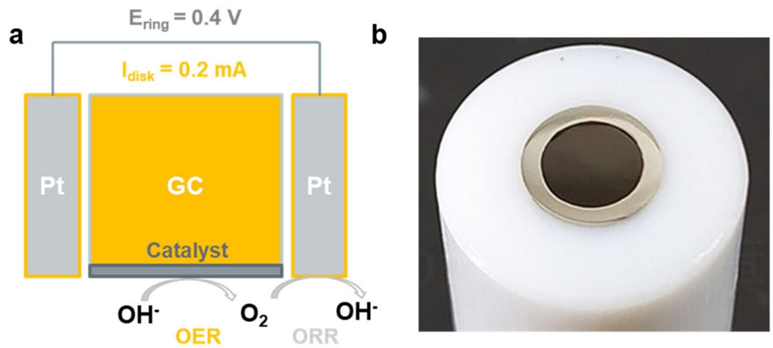

Supplementary Figure 18. The schematic diagram created in Microsoft PowerPoint of the reactions (**a**) using RRDE (**b**) during the FE test.

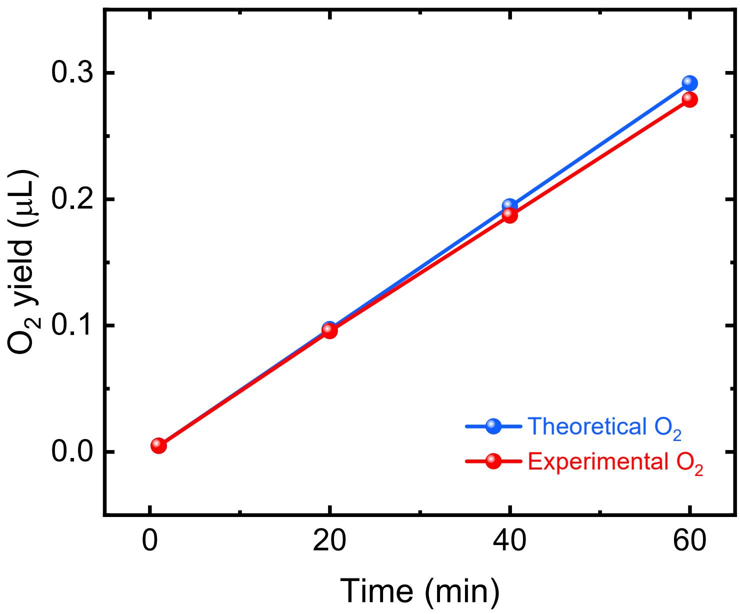

Supplementary Figure 19. The experimental and theoretical oxygen yield, calculated by Faradic efficiency (FE). Source data are provided as a Source Data file.

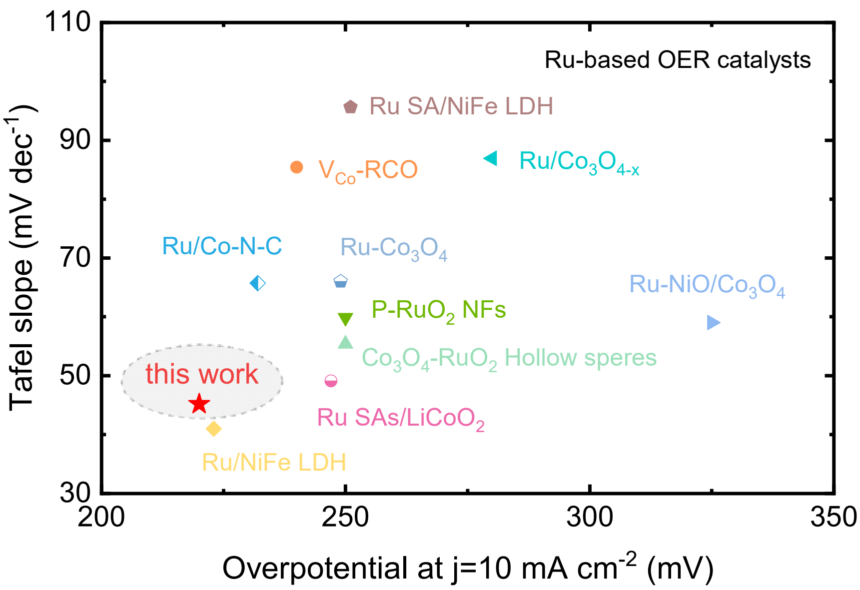

Supplementary Figure 20. Comparison of the Tafel slopes and overpotentials in reported Ru-based OER electrocatalysts. [1, 2, 3, 4, 5, 6, 7, 8, 9, 10]

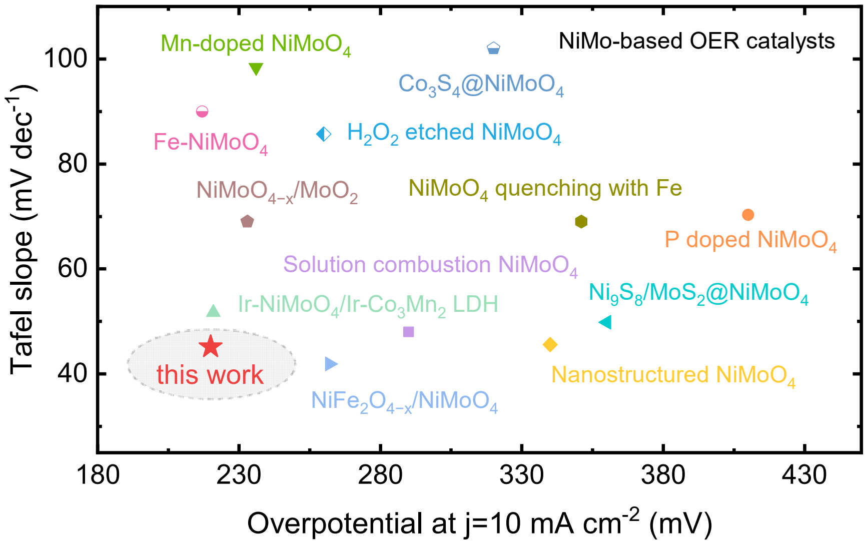

Supplementary Figure 21. Comparison of the Tafel slopes and overpotentials in reported NiMo-based oxide OER electrocatalysts. [11, 12, 13, 14, 15, 16, 17, 18, 19, 20, 21, 22, 23]

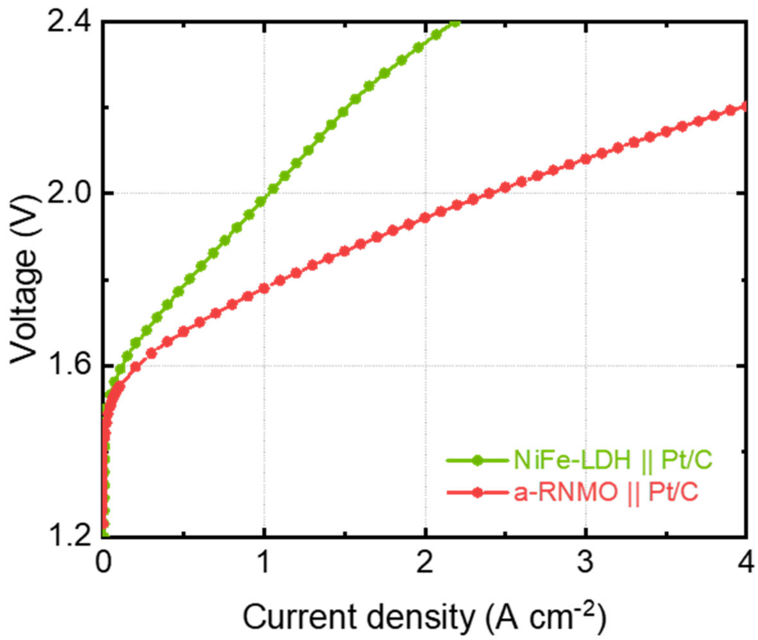

Supplementary Figure 22. AEMWE polarization curve of the electrolyzer without iR correction using a-RNMO or NiFe-LDH as the anode and Pt/C as the cathode. Source data are provided as a Source Data file.

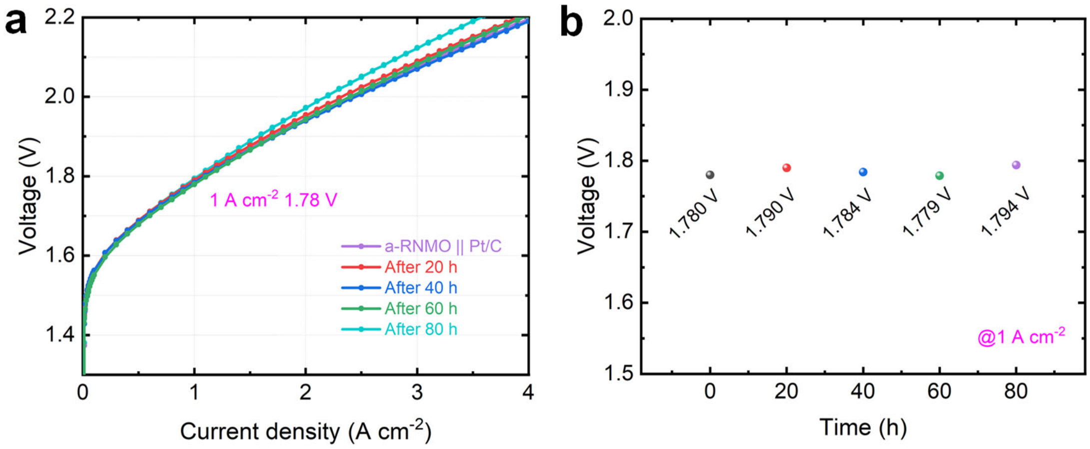

Supplementary Figure 23. AWMWE system of (**a**) polarization curves without *iR* correction and (**b**) voltage at 1 A cm^{-2} during durability with a-RNMO as the anode and Pt/C as the cathode. Source data are provided as a Source Data file.

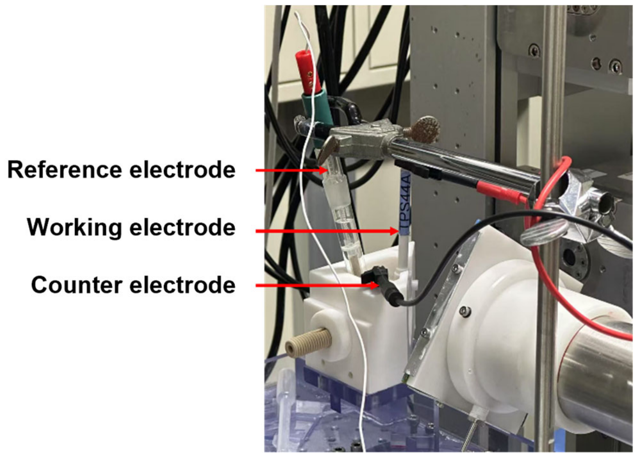

Supplementary Figure 24. The setup of the time-revolved operando XAS test.

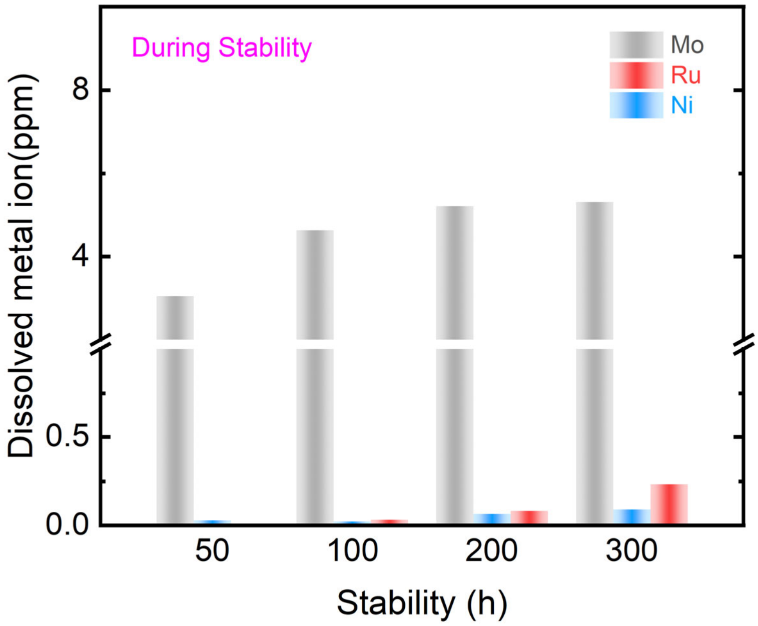

Supplementary Figure 25. The dissolved amounts, by ICP-MS measurements, of Mo, Ru, and Ni ions during the durability test. Source data are provided as a Source Data file.

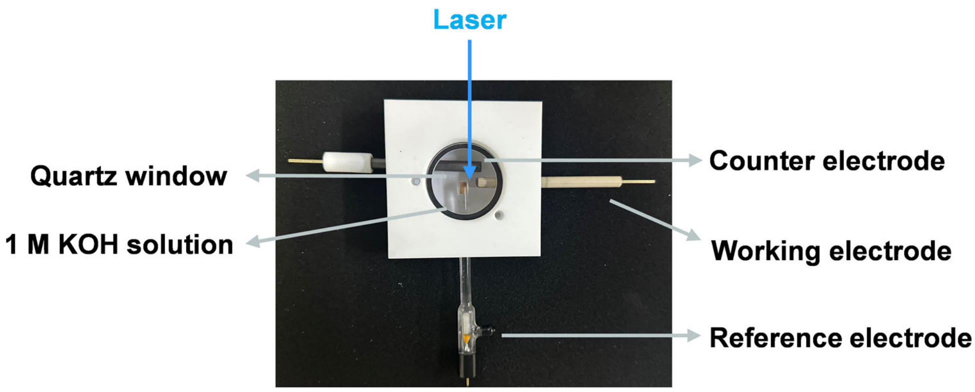

Supplementary Figure 26. The electrochemical cell device of the operando Raman test.

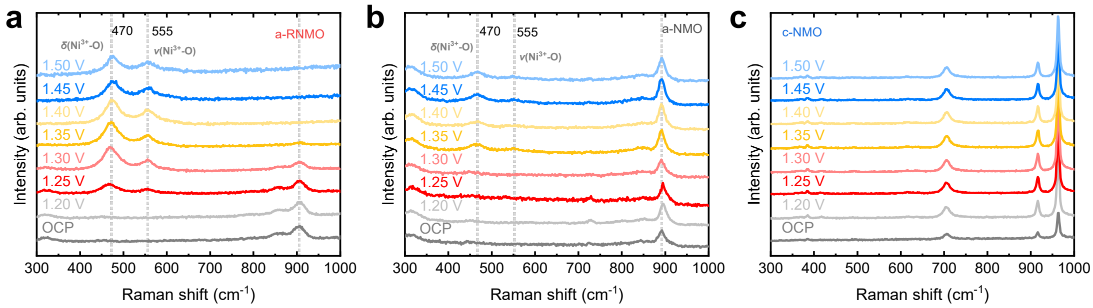

Supplementary Figure 27. Raman spectra of (**a**) a-RNMO and (**b**) a-NMO, and (**c**) c-NMO measured in 1 M KOH under OCP, and OER operating condition (from 1.20 V to 1.50 V vs. RHE). Source data are provided as a Source Data file.

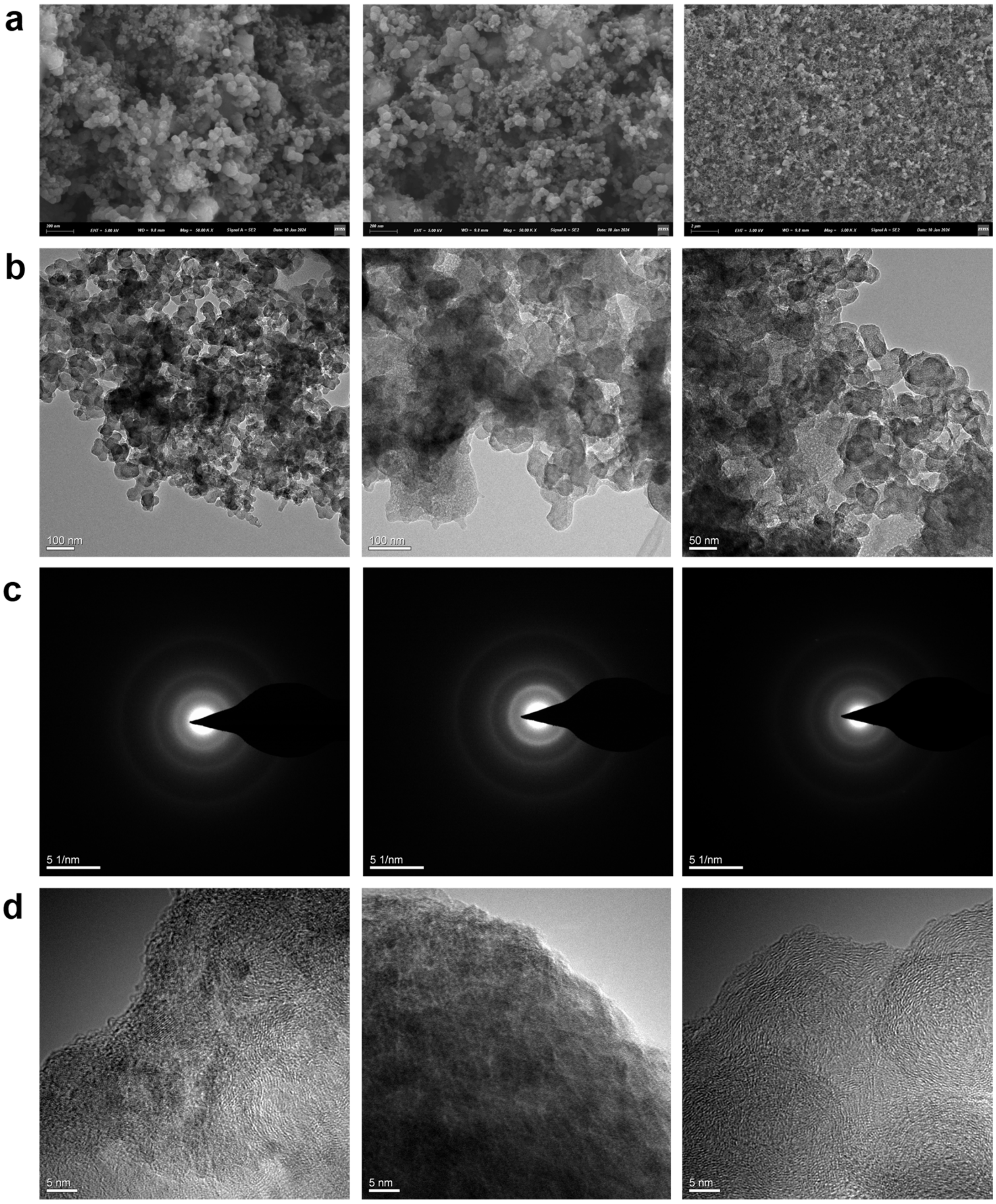

Supplementary Figure 28. (**a**) SEM, (**b**) TEM, and (**c**) SAED, (**d**) HR-TEM images of a-RNMO after OER operation.

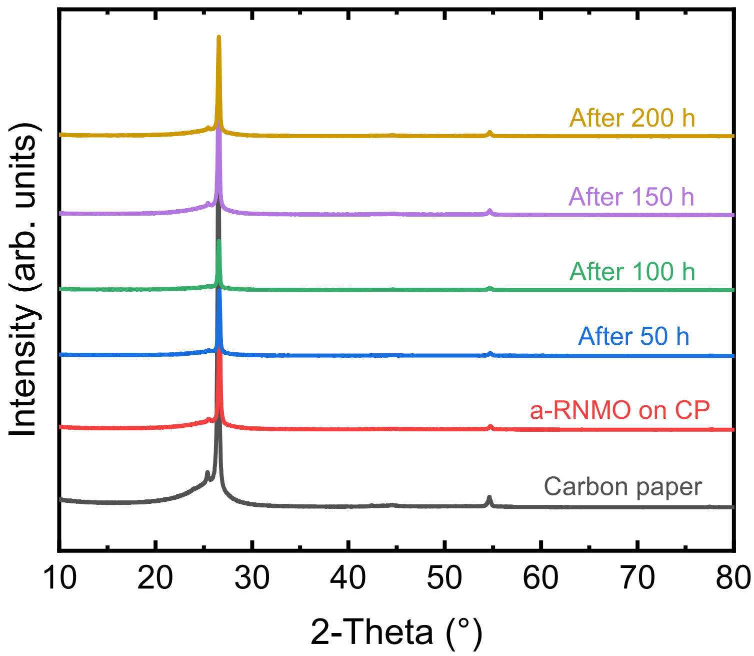

Supplementary Figure 29. XRD patterns of a-RNMO during 200 h OER stability. Source data are provided as a Source Data file.

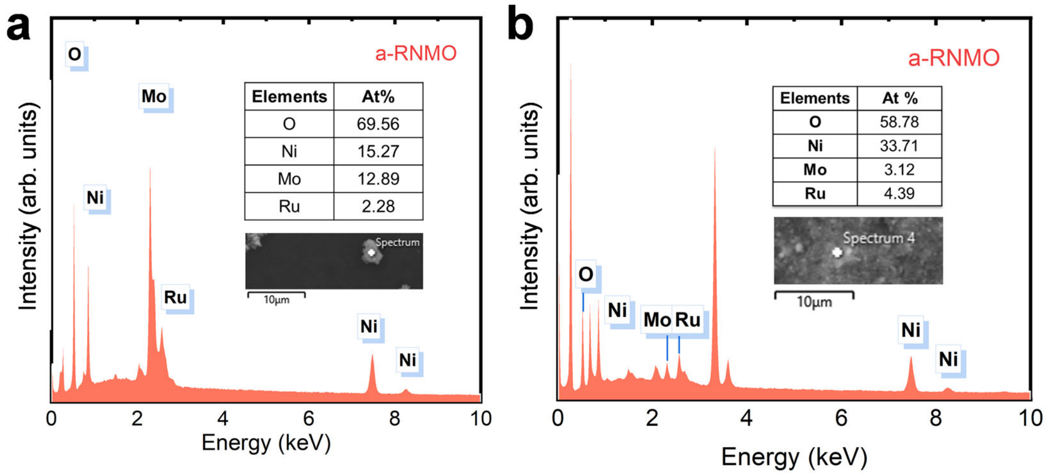

Elements	At%
O	69.56
Ni	15.27
Mo	12.89
Ru	2.28

Elements	At %
O	58.78
Ni	33.71
Mo	3.12
Ru	4.39

Supplementary Figure 30. SEM-EDS spectrum of (**a**) pristine a-RNMO and (**b**) after OER operation. Source data are provided as a Source Data file.

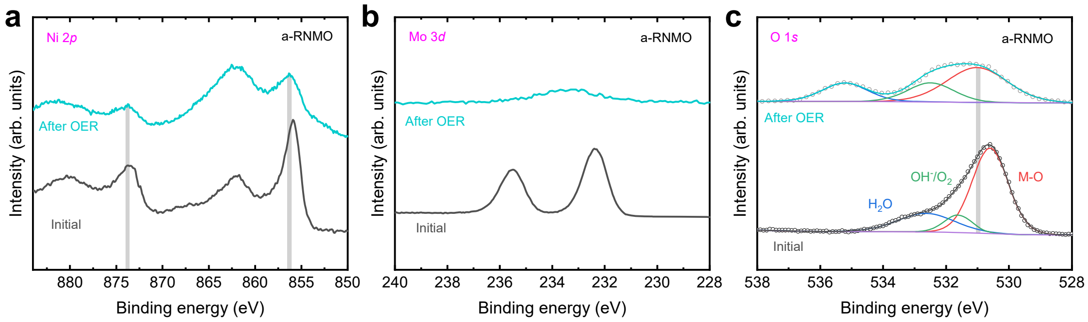

Supplementary Figure 31. XPS spectrum of a-RNMO with (**a**) Ni 2*p*, (**b**) Mo 3*d*, and (**c**) O 1*s* before and after stability test. Source data are provided as a Source Data file.

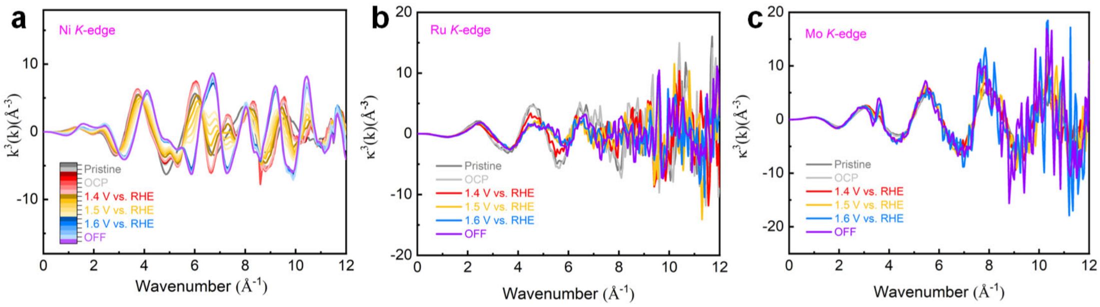

Supplementary Figure 32. The k^3-weighted k-space of (**a**) Ni *K*-edge, (**b**) Ru *K*-edge, and (**c**) Mo *K*-edge experimental spectra of a-RNMO. Source data are provided as a Source Data file.

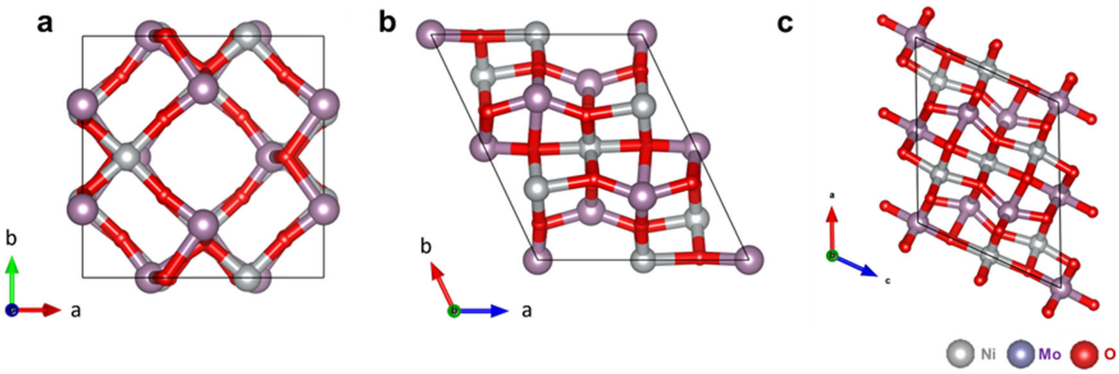

Supplementary Figure 33. Crystal model about c-NMO with three different projection directions.

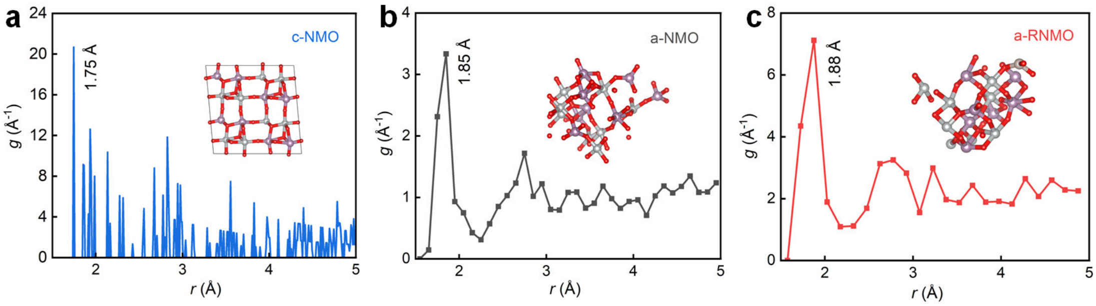

Supplementary Figure 34. PDF results from theoretical simulations, corresponding (**a**) c-NMO, (**b**) a-NMO, and (**c**) a-RNMO. Source data are provided as a Source Data file.

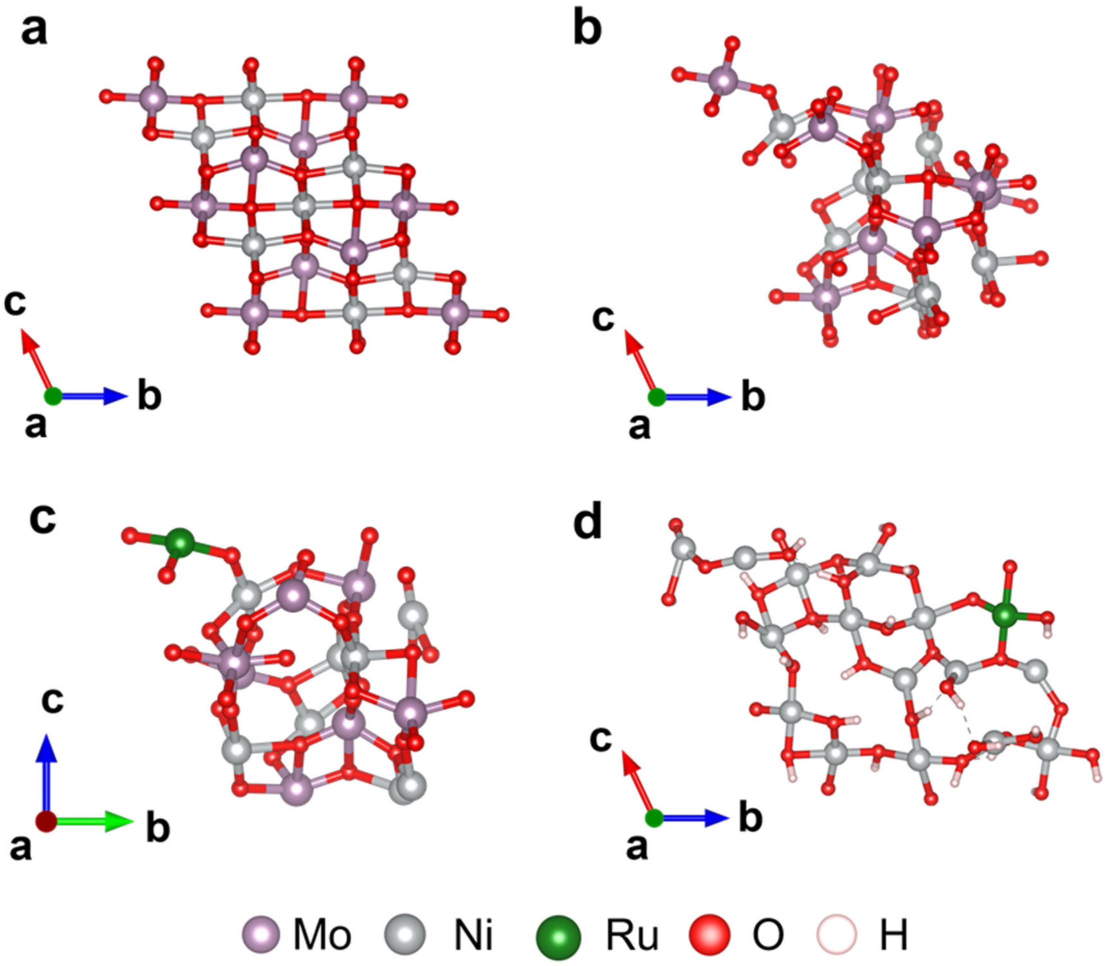

Supplementary Figure 35. The POSCAR details of (**a**) c-NMO, (**b**) a-NMO, (**c**) a-RNMO, and (**d**) a-Ru/NiOOH.

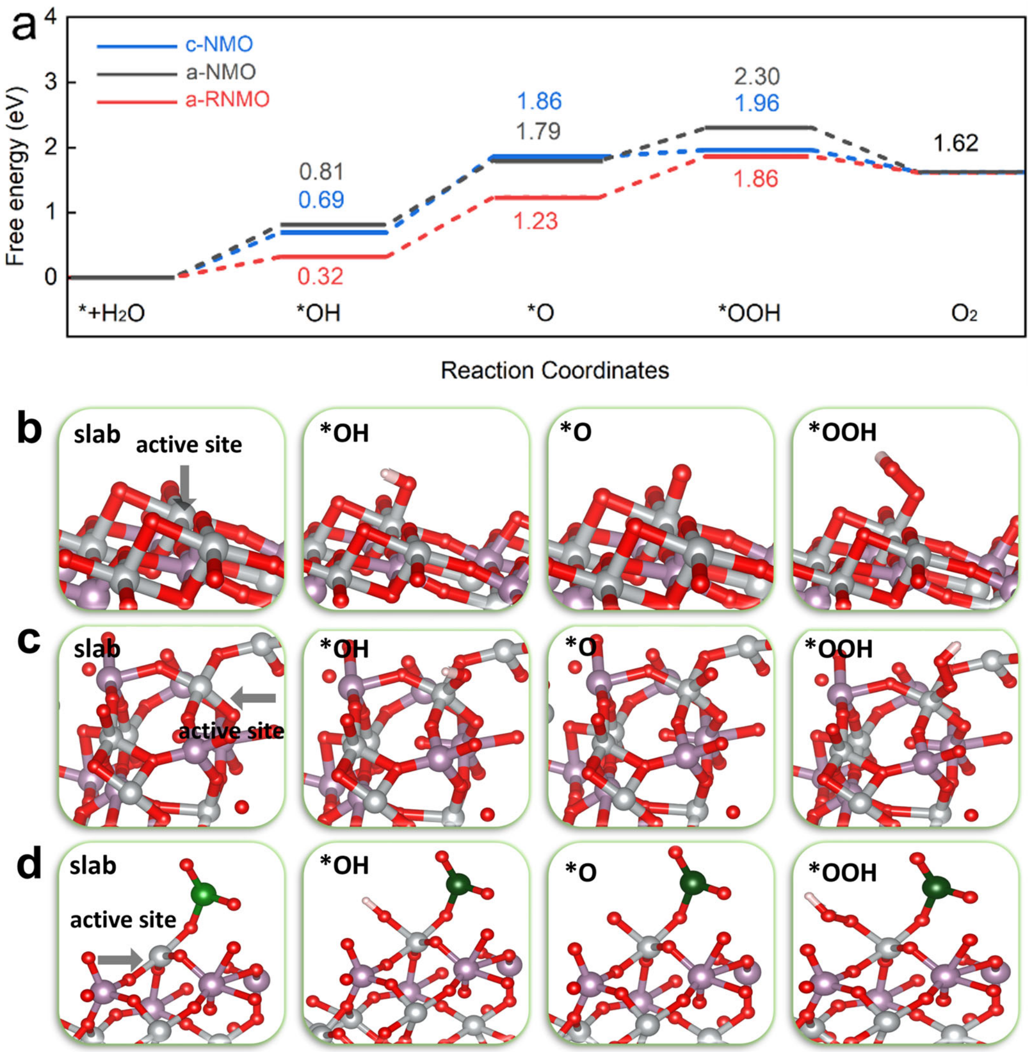

Supplementary Figure 36. (a) Gibbs free energy diagram for the four steps of the OER process (U=0 V). (b-d) The corresponding models of oxygen intermediates during OER process, such as *OH, *O, and *OOH of (b) c-NMO, (c) a-NMO, and (d) a-RNMO. The Ni ion in the (-112) crystal plane was the active site. The red, grey, purple, and green spheres represent O, Ni, Mo, and Ru, respectively. Source data are provided as a Source Data file.

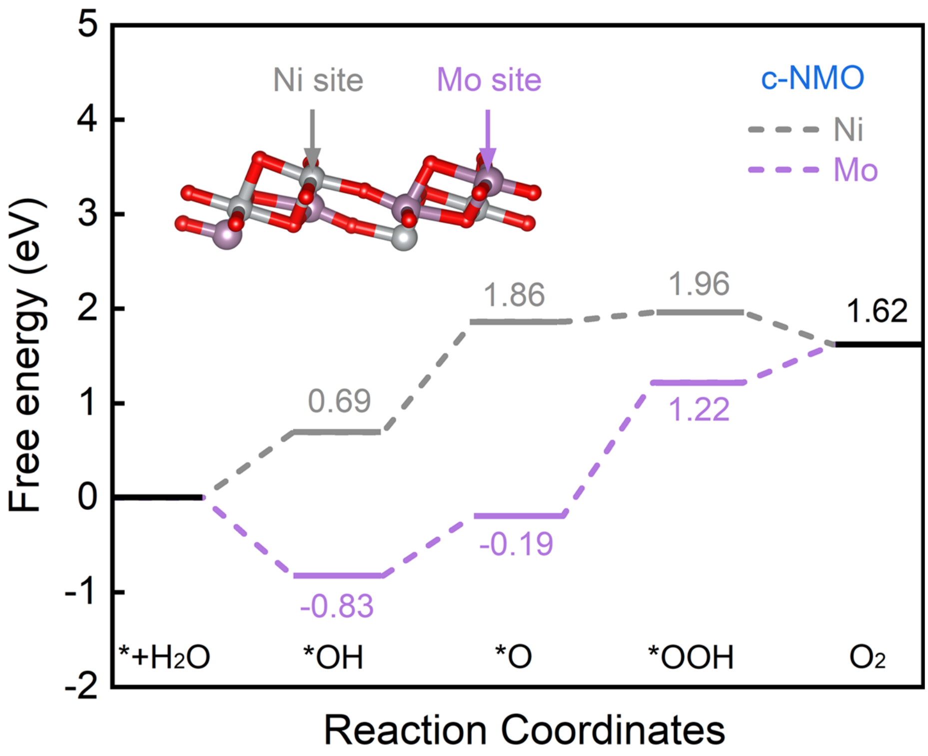

Supplementary Figure 37. Free energy results on the most stable crystal plane (-112) about c-NMO, including Ni sites and Mo sites, respectively (U=0 V). Source data are provided as a Source Data file.

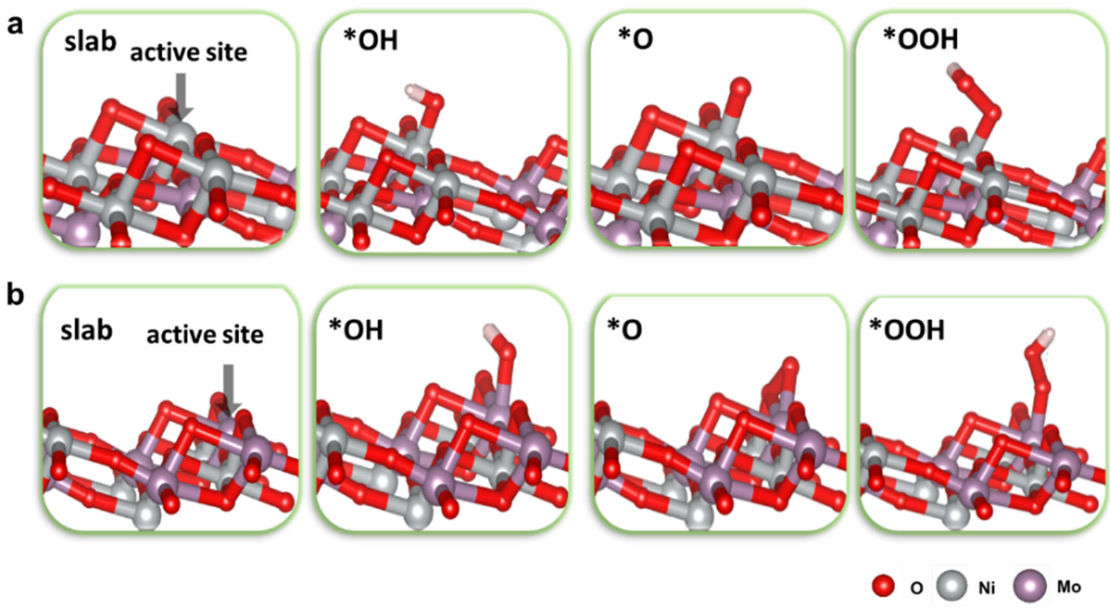

Supplementary Figure 38. The corresponding models of oxygen intermediates during OER process about c-NMO. (**a**) The Ni ion (grey color) was the active site. (**b**) The Mo ion (purple color) was the active site.

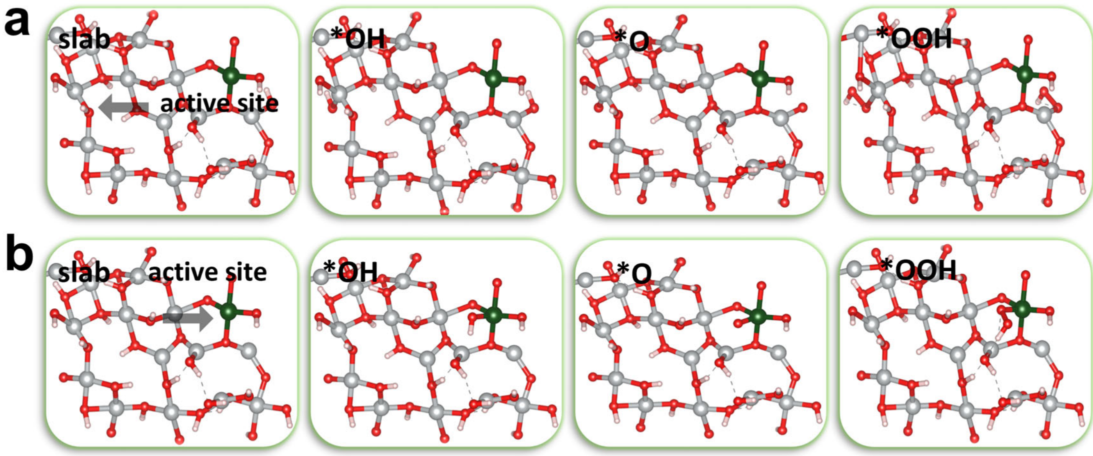

Supplementary Figure 39. The corresponding models of oxygen intermediates during OER process about a-Ru/NiOOH. (**a**) The Ni ion (grey color) was the active site. (**b**) The Ru ion (green color) was the active site.

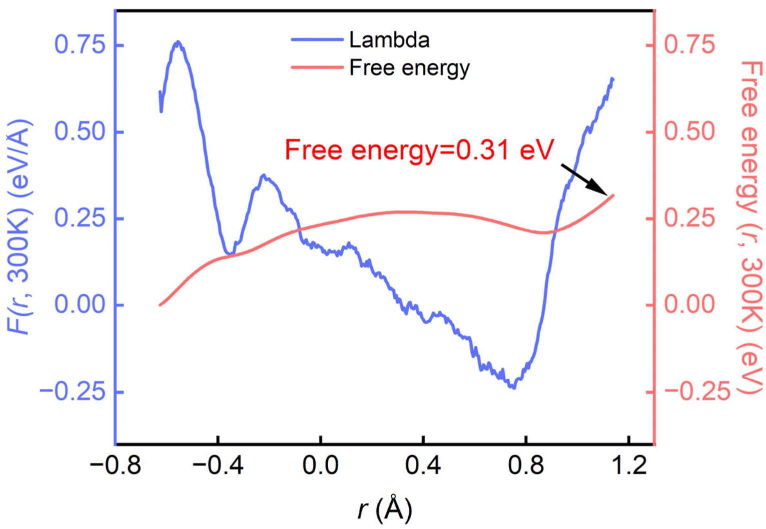

Supplementary Figure 40. Potential of mean force (PMF) profile along the Ru-Ni sites at 300 K. Source data are provided as a Source Data file.

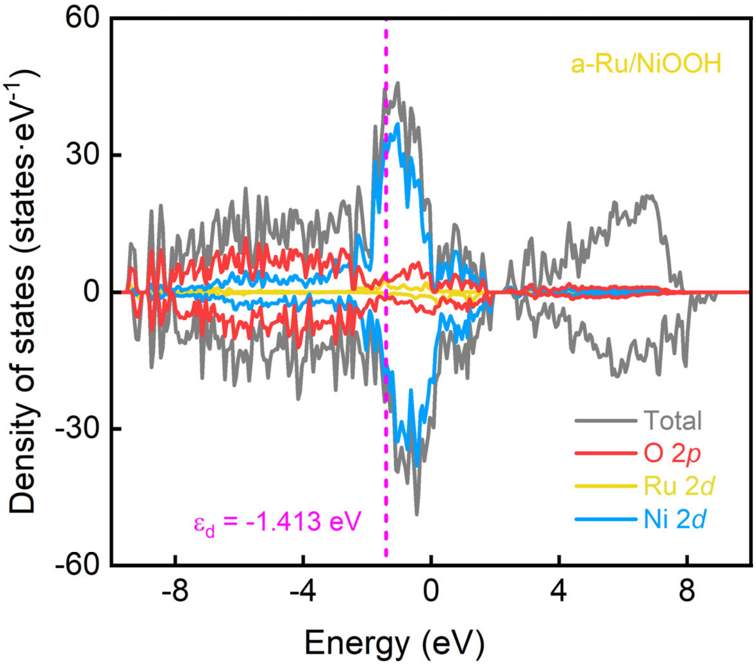

Supplementary Figure 41. Projected density of states (pDOS) curves and *d*-band center of a-Ru/NiOOH. Source data are provided as a Source Data file.

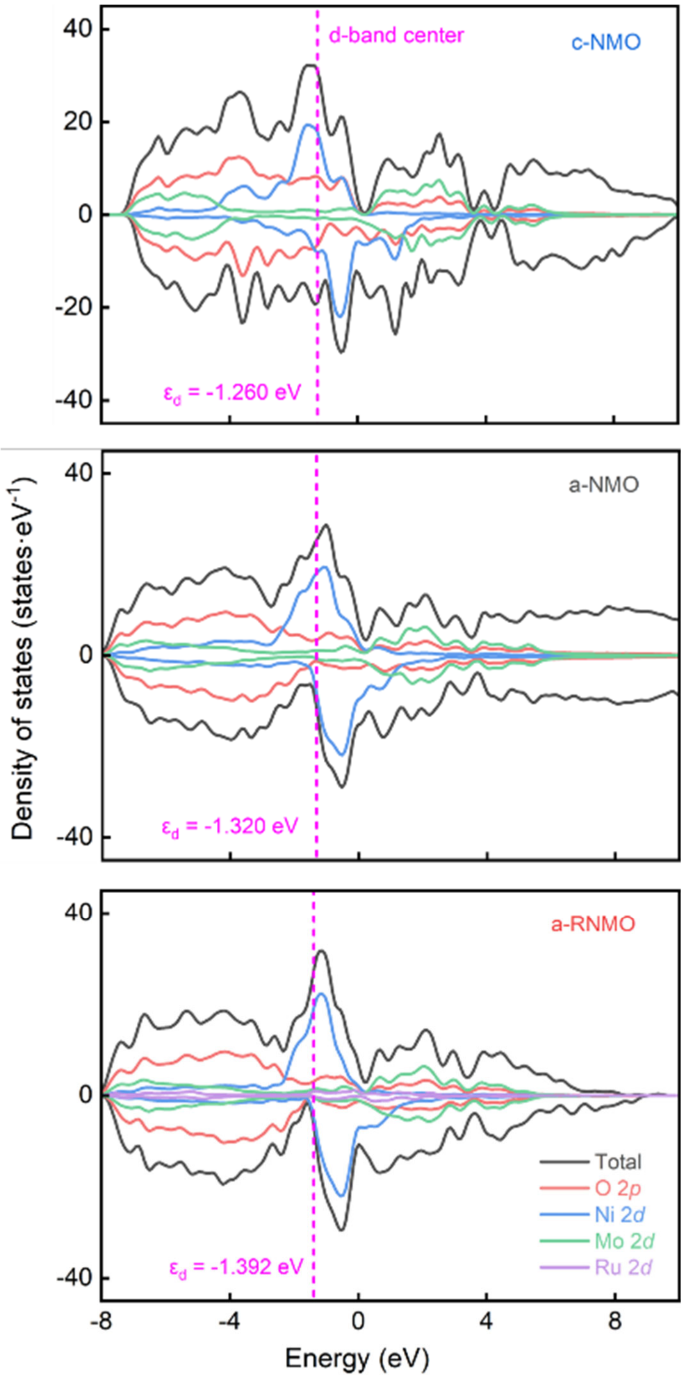

Supplementary Figure 42. DOS curves and *d*-band center of c-NMO, a-NMO, and a-RNMO. Source data are provided as a Source Data file.

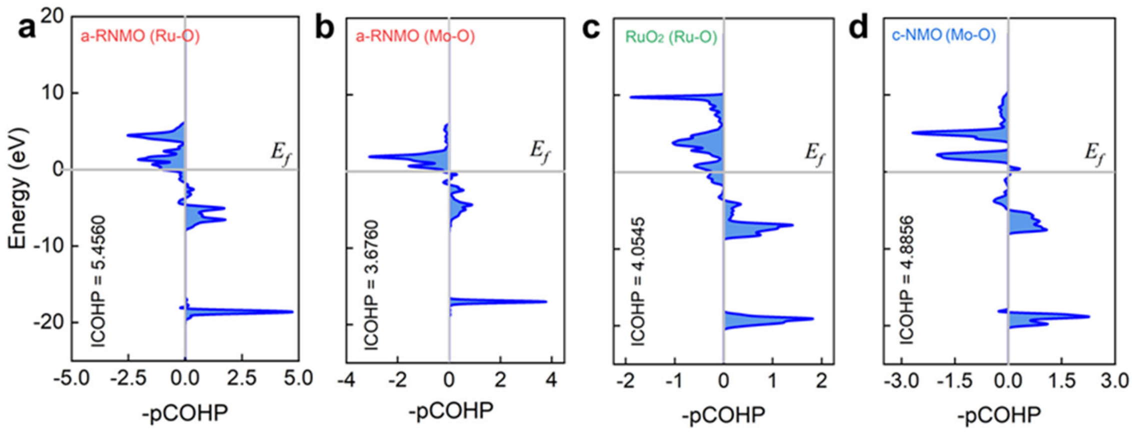

Supplementary Figure 43. The crystal orbital Hamilton populations (COHPs) of (a-b) a-RNMO (Ru-O, and Mo-O), (c) RuO2 (Ru-O), and (d) c-NMO (Mo-O). Source data are provided as a Source Data file.

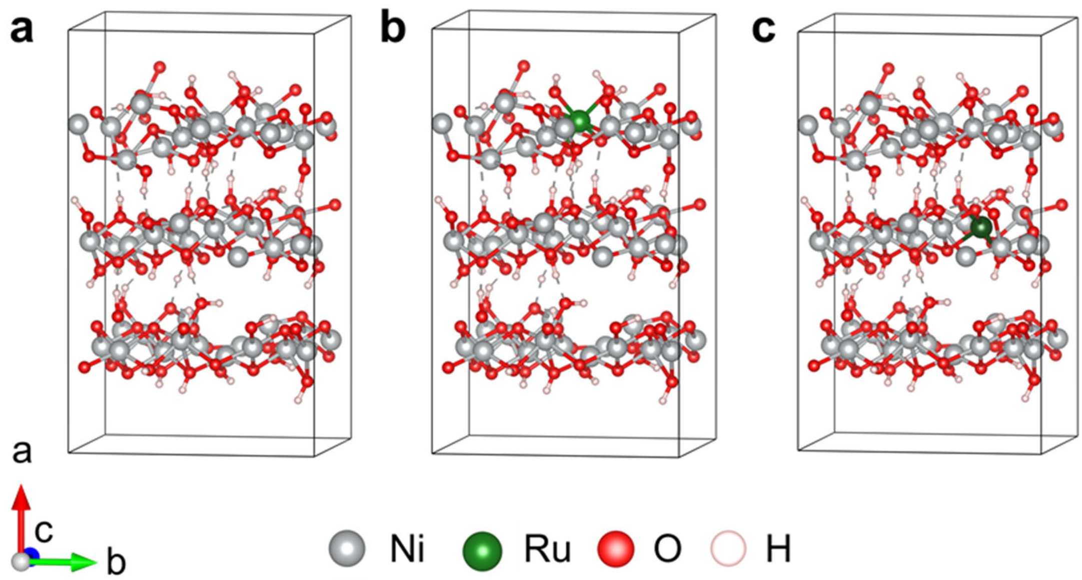

Supplementary Figure 44. The structure models of (a) a-NiOOH, (b) a-Ru/NiOOH, and (c) Ru dopant in a-NiOOH.

Supplementary Tables

Supplementary Table 1. The X-ray PDF refinement results of a-NMO, a-RNMO, and c-NMO. The fitting range is from 1.5 to 10 Å. R_w is the goodness-of-fit parameter. U_{iso} (units of Å^2) is the isotropic atomic displacement parameter (ADP). SPD (units of Å) is the domain size of coherent scattering in the material.

		a-NMO	a-RNMO	c-NMO
R_w		0.2898	0.2497	0.1736
a (Å)		9.7098	8.7164	9.6347
b (Å)		8.1479	8.9606	8.7162
c (Å)		7.6016	7.3537	7.7298
	Ni#1	0.0197	0.0205	0.0024
	Ni#2	0.0073	0.0004	0.0152
U_{iso} (Å^2)	Mo#1	0.0031	0.0055	0.0112
	Mo#2	0.0016	0.0035	0.0018
	O	0.0002	0.0002	0.0006
SPD (Å)		7.8673	8.3899	/

Supplementary Table 2. The Mo/Ni and Ru/Ni molar ratio results by inductively coupled plasma- optical emission spectrometer (ICP-OES) measurement.

Samples (x value)	a-NMO	a-RNMO
Mo/Ni molar ratio	~0.78	~0.75
Ru/Ni molar ratio	N.A.	~0.15

Supplementary Table 3. Fitting parameters of EIS for a-RNMO, a-NMO, c-NMO, and RuO_2.

	R_s (Ohm)	CPE-T	CPE-P	R_{ct} (Ohm)
a-RNMO	5.266±0.075	0.01063±0.00048	0.80525±0.01493	15.33±0.36
a-NMO	4.796±0.054	0.01287±0.00018	0.94058±0.00674	47.82±0.76
c-NMO	5.111±0.084	0.00050±0.000005	0.92376±0.00254	890.70±9.86
RuO_2	5.731±0.129	0.00129±0.00003	0.82796±0.00661	101.80±1.18

Supplementary Table 4. The Tafel slopes and overpotentials at 10 mA cm^{-2} of reported Ru-based OER electrocatalysts.

Overpotential at 10 mA cm^{-2}	Tafel slope	Ru-based electrocatalysts	Reference
232	65.7	Ru/Co-N-C	[1]
240	85.4	V_{Co}-RCO	[2]
247	49.1	Ru SAs/$LiCoO_2$	[3]
249	66	Ru-Co_3O_4	[4]
250	55.4	Co_3O_4-RuO_2 Hollow speres	[5]
250	59.9	P-RuO_2 NFs	[6]
251	95.6	Ru SA/NiFe LDH	[7]
280	86.9	Ru/Co_3O_{4-x}	[8]
325	59	Ru-NiO/Co_3O_4	[9]
223	41	Ru/NiFe LDH	[10]
220	45.15	a-RNMO	This work

Supplementary Table 5. The Tafel slopes and overpotentials at 10 mA cm^{-2} of reported NiMo-based oxide OER electrocatalysts.

Overpotential at 10 mA cm^{-2}	Tafel slope	NiMo-based oxide electrocatalysts	Reference
217	90	Fe-$NiMoO_4$ nanotube	[11]
221	51.7	Ir-$NiMoO_4$/Ir-Co_3Mn_2 LDH	[12]
233	69	$NiMoO_{4-x}$/MoO_2	[13]
236	98.4	Mn-doped $NiMoO_4$	[14]
260	85.7	$NiMoO_4$ nanorods etched by H_2O_2	[15]
262	41.9	$NiFe_2O_{4-x}$/$NiMoO_4$	[16]
283	44.3	N-$NiMoO_4$/NiS_2	[17]
290	48	$NiMoO_4$ with solution combustion method	[18]
320	102	Co_3S_4@$NiMoO_4$ nanotube	[19]
340	45.6	Nanostructured $NiMoO_4$	[20]
351	69	$NiMoO_4$ quenching in $Fe(NO_3)_3$ solutions	[21]
360	49.83	Ni_9S_8/MoS_2@$NiMoO_4$	[22]
410	70.3	P doped $NiMoO_4$	[23]
220	45.15	a-RNMO	This work

Supplementary Table 6. The Mo/Ni and Ru/Ni molar ratio results, by ICP-MS measurement, before and after OER process.

Samples (x value)	a-RNMO pristine	a-RNMO after OER
Mo/Ni molar ratio	~0.75	~0.14
Ru/Ni molar ratio	~0.15	~0.14

Supplementary Table 7. The formation enthalpy (E_f) and dissolution potential (U_{diss}) of RuO_2 with Ru, c-NMO with Mo, a-RNMO with Ru and Mo, Ru SAs in a-NiOOH with Ru, and Ru doped in a-NiOOH with Ru.

Ru	Ru_2O_4	Ru2	O2	Ef			Udiss (Ru)	Ne	Udiss
	-44.6142	-18.4695	-9.8577	-6.42935			0.46	2	3.674674
Mo	c-NMO	O2	Ni4	Mo2	Ef		Udiss (Mo)	Ne	Udiss
	-360.883	-9.8577	-21.7879	-21.8608	-9.017579		-0.2	3	2.80586
Ru	a-RNMO	O2	Ni4	Mo2	Ru2	Ef	Udiss (Ru)	Ne	Udiss
	-308.392	-9.8577	-21.7879	-21.8608	-18.4695	-9.49843	0.46	2	5.209216
Mo	a-RNMO	O2	Ni4	Mo2	Ru2	Ef	Udiss (Mo)	Ne	Udiss
	-308.392	-9.8577	-21.7879	-21.8608	-18.4695	-9.49843	-0.2	3	2.966144
Ru	Ru SAs in a-NiOOH	Ru2	Total	Ef			Udiss (Ru)	Ne	Udiss
	-884.4657	-18.4695	-899.925	-6.22405			0.46	2	3.572025
Ru	Ru doped in a-NiOOH	Ru2	Total	Ef			Udiss (Ru)	Ne	Udiss
	-884.9567	-18.4695	-898.838	-4.64695			0.46	2	2.783475

Supplementary Table 8. Zero-point energies about c-NMO, a-NMO, a-RNMO, and a-Ru/NiOOH.

	c-NMO		
	*OH	*O	*OOH
Ni active site	0.31	0.03	0.36
Mo active site	0.27	0.03	0.33
	a-NMO		
	*OH	*O	*OOH
Ni active site	0.3	0.01	0.34
	a-RNMO		
	*OH	*O	*OOH
Ni active site	0.29	0.01	0.35
Ru active site	-0.27	0.05	0.35
	a-Ru/NiOOH		
	*OH	*O	*OOH
Ni active site	0.29	0.01	0.35
Ru active site	-0.28	0.05	0.35

Supplementary References

1. Rong C, *et al.* Electronic Structure Engineering of Single-Atom Ru Sites via Co–N_4 Sites for Bifunctional pH-Universal Water Splitting. *Adv. Mater.* **34**, 2110103 (2022).
2. Pan S, *et al.* Neighboring Site Synergies in Co-Defective Ru–Co Spinel Oxide toward Oxygen Evolution Reaction. *ACS Sustain. Chem. Eng.* **11**, 290-299 (2023).
3. Zheng X, *et al.* Ru–Co Pair Sites Catalyst Boosts the Energetics for the Oxygen Evolution Reaction. *Angew. Chem. Int. Ed.* **61**, e202205946 (2022).
4. Zhao C, *et al.* Insights into the electronic origin of enhancing the catalytic activity of Co_3O_4 for oxygen evolution by single atom ruthenium. *Nano Today* **34**, 100955 (2020).
5. Gao Y, *et al.* 3D Co_3O_4-RuO_2 Hollow Spheres with Abundant Interfaces as Advanced Trifunctional Electrocatalyst for Water-Splitting and Flexible Zn–Air Battery. *Adv. Funct. Mater.* **32**, 2203206 (2022).
6. Zhang L, Li W, Ren S, Song W, Wang C, Lu X. Manipulating d-Band Center of Ru Sites in Branched RuO_2 Nanofibers Enables Significantly Enhanced Alkaline Overall Water Splitting Performance. *Adv. Energy Mater.* **15**, 2403136 (2025).
7. Yang Y, *et al.* Enhancing Water Oxidation of Ru Single Atoms via Oxygen-Coordination Bonding with NiFe Layered Double Hydroxide. *ACS Catal.* **13**, 2771-2779 (2023).
8. Yuan C-Z, *et al.* In Situ Immobilizing Atomically Dispersed Ru on Oxygen-Defective Co_3O_4 for Efficient Oxygen Evolution. *ACS Catal.* **13**, 2462-2471 (2023).
9. Zhang J, Lian J, Jiang Q, Wang G. Boosting the OER/ORR/HER activity of Ru-doped Ni/Co oxides heterostructure. *Chem. Eng. J.* **439**, 135634 (2022).
10. Zhai P, *et al.* Engineering single-atomic ruthenium catalytic sites on defective nickel-iron layered double hydroxide for overall water splitting. *Nat. Commun.* **12**, 4587 (2021).
11. Yin Z, *et al.* Hybrid-atom-doped $NiMoO_4$ nanotubes for oxygen evolution reaction. *New J. Chem.* **44**, 17477-17482 (2020).
12. Tang S, *et al.* Surface/interface engineering for fabricating hierarchical Ir doped $NiMoO_4$ covered by CoMn layered double hydroxide toward oxygen evolution reaction. *J. Alloys Compd.* **924**, 166415 (2022).
13. Zhang Z, Ma X, Tang J. Porous $NiMoO_{4-x}$/MoO_2 hybrids as highly effective electrocatalysts for

the water splitting reaction. *J. Mater. Chem. A* **6**, 12361-12369 (2018).

14. Yang S*, et al.* In Situ Fabrication of Mn-Doped $NiMoO_4$ Rod-like Arrays as High Performance OER Electrocatalyst. *Nanomaterials* **13**, 827 (2023).
15. Zhu J, Qian J, Peng X, Xia B, Gao D. Etching-Induced Surface Reconstruction of $NiMoO_4$ for Oxygen Evolution Reaction. *Nano-Micro Lett.* **15**, 30 (2023).
16. Choi J*, et al.* Interface engineered $NiFe_2O_{4-x}$/$NiMoO_4$ nanowire arrays for electrochemical oxygen evolution. *Appl. Catal. B: Environ.* **286**, 119857 (2021).
17. An L*, et al.* Epitaxial Heterogeneous Interfaces on N-$NiMoO_4$/NiS_2 Nanowires/Nanosheets to Boost Hydrogen and Oxygen Production for Overall Water Splitting. *Adv. Funct. Mater.* **29**, 1805298 (2019).
18. Rammal MB, Omanovic S. Synthesis and characterization of NiO, MoO_3, and $NiMoO_4$ nanostructures through a green, facile method and their potential use as electrocatalysts for water splitting. *Mater. Chem. Phys.* **255**, 123570 (2020).
19. Chen L, Xu GC, Xu G, Zhang L, Ding H. Co-based coordination polymer-derived Co_3S_4 nanotube decorated with NiMoO4 nanosheets for effective oxygen evolution reaction. *Int. J. Hydrogen Energy* **45**, 30463-30472 (2020).
20. Zhao X, Meng J, Yan Z, Cheng F, Chen J. Nanostructured $NiMoO_4$ as active electrocatalyst for oxygen evolution. *Chin. Chem. Lett.* **30**, 319-323 (2019).
21. Ye C*, et al.* Activating Metal Oxides Nanocatalysts for Electrocatalytic Water Oxidation by Quenching-Induced Near-Surface Metal Atom Functionality. *J. Am. Chem. Soc.* **143**, 14169-14177 (2021).
22. Kang J*, et al.* Valence oscillation and dynamic active sites in monolayer NiCo hydroxides for water oxidation. *Nat. Catal.* **4**, 1050-1058 (2021).
23. Zhang S, She G, Li S, Qu F, Mu L, Shi W. Enhancing the electrocatalytic activity of $NiMoO_4$ through a post-phosphorization process for oxygen evolution reaction. *Catal. Commun.* **129**, 105725 (2019).